

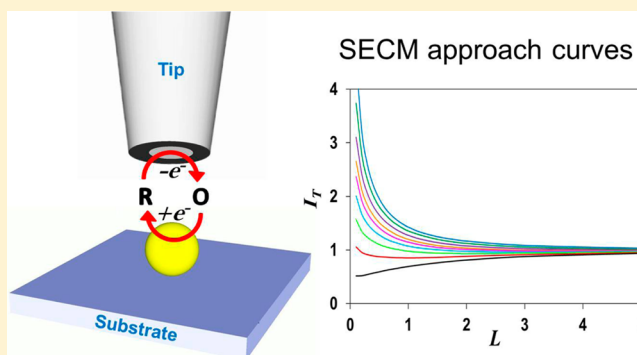
Scanning Electrochemical Microscopy of Single Spherical Nanoparticles: Theory and Particle Size Evaluation

Yun Yu, Tong Sun, and Michael V. Mirkin*

Department of Chemistry and Biochemistry, Queens College - CUNY, Flushing, New York 11367, United States
The Graduate Center, City University of New York, New York, New York 10016, United States

S Supporting Information

ABSTRACT: Experiments at individual metal nanoparticles (NPs) can provide important information about their electrochemical and catalytic properties. The scanning electrochemical microscope (SECM) equipped with a nanometer-sized tip was recently used to image single 10 or 20 nm gold particles and quantitatively investigate electrochemical reactions occurring at their surfaces. In this Article, the theory is developed for SECM current vs distance curves obtained with a disk-shaped tip approaching a comparably sized, surface-bound conductive or insulating spherical NP. The possibility of evaluating the size of a surface-bound particle by fitting the experimental current–distance curve to the theory is shown for NPs and tips of different radii. The effects of the NP being partially buried into an insulating layer and the imperfect positioning of the tip with respect to the NP center are considered. The collection efficiency is calculated for redox species generated at the nanoparticle surface and collected at the tip.



Electrochemical processes involving nanoparticles (NPs) have been the subject of extensive research because of their extraordinary physical and chemical properties^{1,2} and applications in sensing³ and electrocatalysis.⁴ The strong size and shape dependence of NP properties is important for various processes from catalysis⁵ to deoxygenation⁶ to NP uptake into mammalian cells.⁷ The effects of variations in individual NP properties are difficult to assess in studies of large ensembles of particles. Thus, several methodologies were developed for electrochemical experiments at single NPs, including optical techniques, such as surface plasmon resonance imaging⁸ and single molecule fluorescence imaging,⁹ and electrochemical measurements at a metal NP either landing at or attached to a small electrode.^{5a,10–16}

We showed recently¹⁷ that electrochemical activity of single gold nanoparticles (AuNPs) attached to the catalytically inert carbon surface can be mapped by using small (≥ 3 nm radius) polished nanoelectrodes as tips in the scanning electrochemical microscope (SECM). Unlike the techniques based on immobilization of single NPs on nanoelectrodes, this approach is potentially useful for studying the effects of nanoparticle size, geometry, and surface attachment in a real-world application environment.

Most of the existing SECM theory was developed for the disk-shaped tip and flat substrate.^{18a} Some approximations and numerical simulations were reported for hemispherical and sphere-cap shaped tips,^{18b–h,19,20a} and only a few curves have been simulated for nonflat substrates and those including microscopic spherical features.^{19,20} Here, we develop the theory

for SECM current–distance curves obtained with a disk-shaped tip approaching a surface-bound spherical NP and calculate the collection efficiency for the electroactive species generated at the spherical substrate and collected at the tip. A schematic representation of the problem geometry used in our finite-element simulations is shown in Figure 1.

An important issue in experiments with single NPs is the particle size evaluation. Several techniques such as dynamic light scattering, nanoparticle tracking analysis, resistive-pulse measurements with nanopores²¹ or nanopipettes,²² NMR spectroscopy,²³ and capillary electrophoresis/inductively coupled plasma mass spectrometry combination²⁴ are available for evaluating the size of NPs in solution. Electron microscopy (especially transmission electron microscopy, TEM) is widely used for measuring dry NP size in vacuum. However, measuring an individual surface-bound NP in an electrochemical system is not straightforward. The ability to evaluate the size of the specific surface-bound particle is essential for electrochemical experiments at the level of single NPs, especially for polydisperse NPs and soft particles whose size in solution can be different from that in vacuum. Atomic force microscopy (AFM) that can visualize a surface-attached NP in solution is prone to greatly overestimating the lateral particle size due to the tip convolution effect,^{17,25} while significant errors in the NP height can result from the tip/sample

Received: May 4, 2015

Accepted: June 23, 2015

Published: July 7, 2015



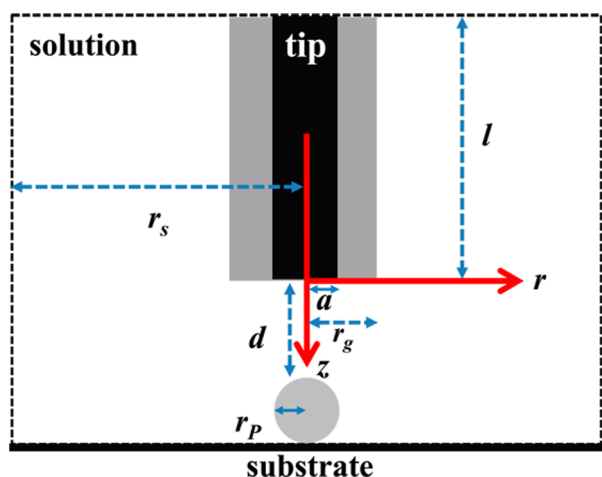


Figure 1. Geometry of the simulation space and parameters defining the diffusion problem for the disk-shaped SECM tip approaching a spherical particle attached to a planar support.

interactions.²⁶ In our recent experiments, the apparent size of 10–20 nm Au NPs was much closer to their nominal diameter in SECM images than in AFM images.¹⁷ However, an SECM image of an NP is relatively hard to obtain and analyze. A more straightforward and accurate approach developed in this Article is based on the fitting of an experimental current vs distance curve to the theory, using the NP radius (r_p) as an adjustable parameter.

In a feedback mode SECM experiment, the electrolyte contains an electroactive species that is oxidized (or reduced) at the tip electrode. When the tip is brought near a conductive substrate, the product of the tip reaction diffuses to its surface, where it gets rereduced (or reoxidized). The tip current increases with decreasing separation distance (d) due to the mediator regeneration process (positive feedback). No mediator regeneration occurs at the insulating substrate, and the tip current decreases with decreasing d because of hindered diffusion of redox species (negative feedback). Several combinations of reactive or inert NPs with either conductive or insulating substrate surfaces can be employed for NP size evaluation: i.e., (1) reactive NP/insulating substrate, (2) inert NP/conductive substrate, (3) reactive NP/conductive substrate, and (4) inert NP/insulating substrate. The first two combinations should be advantageous because of the sharp contrast between the positive feedback produced by the reactive NP and negative feedback at the underlying insulating surface (or vice versa in case 2). Because electrochemical experiments typically employ reactive (i.e., metal) NPs, our primary focus here is on combination (1). To regenerate the redox mediator, a particle with r_p comparable to the tip radius (a) must be electrically connected. For the conductive NP/insulating substrate combination, this can be attained either by partially burying a NP into a nm-thick passivating film (e.g., a polyphenylene multilayer electrografted to a conductive graphite surface¹⁷) or via the electron tunneling between the NP and the underlying conductive surface through the insulating film.^{11c,27}

THEORY

Feedback Mode. The steady-state diffusion problem formulated below applies to the SECM feedback mode with a one-step electron transfer reaction occurring at the disk-shaped

tip. The tip is held at a potential (E_T) at which the oxidation (or the reduction) of the solution species is diffusion limited. The spherical object is immobilized on the plane, and the mediator regeneration occurs at the conductive portion of the substrate (either a NP or the surrounding planar surface) at the diffusion-controlled rate. With the excess supporting electrolyte, the corresponding differential equation in cylindrical coordinates is

$$\frac{\partial^2 c}{\partial r^2} + \frac{1}{r} \frac{\partial c}{\partial r} + \frac{\partial^2 c}{\partial z^2} = 0 \quad (1)$$

where r and z are the spatial coordinates (Figure 1) and $c(r, z)$ is the concentration of redox species.

The dimensionless variables can be introduced as follows:

$$R = r/a \quad (2a)$$

$$Z = z/a \quad (2b)$$

$$C(R, Z) = c(r, z)/c^* \quad (2c)$$

$$LL = l/a \quad (2d)$$

$$RG = r_g/a \quad (2e)$$

$$RS = r_s/a \quad (2f)$$

$$L = d/a \quad (2g)$$

$$RP = r_p/a \quad (2h)$$

where c^* is the bulk concentration, r_g is the tip insulator radius, r_s is the simulation space limit in the radial direction, l is the z -coordinate of the lower simulation space limit, and d is the vertical distance from the tip to the sphere top. The current was calculated by solving the following diffusion problem in the dimensionless form:

$$\frac{\partial^2 C}{\partial R^2} + \frac{1}{R} \frac{\partial C}{\partial R} + \frac{\partial^2 C}{\partial Z^2} = 0; \quad 0 \leq R < RS, -LL < Z < 2RP + L \quad (3)$$

$$C = 0; \quad 0 \leq R \leq 1, Z = 0 \text{ (tip surface)} \quad (4)$$

One of two following conditions is applicable to either reactive (eq 5a) or inert (eq 5b) NP:

$$C = 1; \quad 0 \leq R \leq RP, Z = L + RP \pm \sqrt{RP^2 - R^2} \text{ (reactive sphere)} \quad (5a)$$

$$\frac{\partial C(R, Z)}{\partial n} = 0; \quad 0 \leq R \leq RP, Z = L + RP \pm \sqrt{RP^2 - R^2} \text{ (inert sphere)} \quad (5b)$$

where $\partial C(R, Z)/\partial n$ is the normal derivative.

One of two following conditions is applicable to either conductive (eq 6a) or insulating (eq 6b) substrate surface:

$$C = 1; \quad 0 < R \leq RS, Z = L + 2RP \text{ (conductive substrate)} \quad (6a)$$

$$\frac{\partial C(R, Z)}{\partial n} = 0; \quad 0 < R \leq RS, Z = L + 2RP \text{ (insulating substrate)} \quad (6b)$$

$$\frac{\partial C(R, Z)}{\partial n} = 0; \quad Z = 0, 1 < R \leq RG; -LL \leq Z \leq 0, \quad R = RG \text{ (insulating region)} \quad (7)$$

$$C = 1; \quad -LL \leq Z \leq 2RP + L, R = RS; Z = -LL, RG < R \leq RS \text{ (simulation space limit)} \quad (8)$$

$$\frac{\partial C(R, Z)}{\partial R} = 0; \quad R = 0, 0 \leq Z \leq L \text{ (axis of symmetry)} \quad (9)$$

The dimensionless tip current obtained by integrating the dimensionless diffusion flux over the tip surface corresponds to the physical current normalized by the diffusion limiting current to the inlaid disk with the radius a .

$$I_T = \frac{i_T}{i_{T,\infty}} = \frac{\pi}{2} \int_0^1 R \left[\frac{\partial C(R, Z)}{\partial Z} \right] dR \quad (10)$$

where

$$i_{T,\infty} = 4nFDc^*a \quad (11)$$

n is the number of transferred electrons, F is Faraday constant, and D is the diffusion coefficient of redox species.

The above diffusion problem was solved numerically using COMSOL Multiphysics version 4.4 commercial simulation package. The shape of the current–distance curves is determined by three dimensionless parameters, $L = d/a$, $RG = r_g/a$, and $RP = r_p/a$. To limit the number of simulations, the theory is developed here only for $RG = 10$. The computed working curves are sufficiently accurate for any RG when the particle is reactive and may contain some error when the NP is inert and $RG \ll 10$.^{18a} Figure 2A presents the I_T vs L dependences for reactive NPs with different RP values immobilized on the insulating substrate (the numerical simulated data is summarized in Table S1 in the Supporting Information). With the increasing RP value, the SECM response changes from pure negative feedback ($RP = 0$; lower dashed curve) to pure positive feedback ($RP = \infty$; upper dashed curve). Similarly to the approach curves calculated earlier for a finite-size disk-shaped conductive substrate embedded into the insulating plane,²⁸ the smallest radius of the reactive spherical NP that can be confidently detected is $\sim 0.1a$ (the bottom solid curve in Figure 2A). The opposite extreme is a large NP (e.g., $RP = 2$; top solid curve) for which the shape of the approach curve is similar to that for a flat conductive substrate (upper dashed curve).

An analytical approximation was derived to facilitate the fitting of experimental approach curves to the theory. The whole family of SECM working curves shown in Figure 2A for $0.1 \leq L \leq 5$ can be accurately described by eq 12.

$$I_T = \frac{a + cL + eL^2}{1 + bL + dL^2} \quad (12)$$

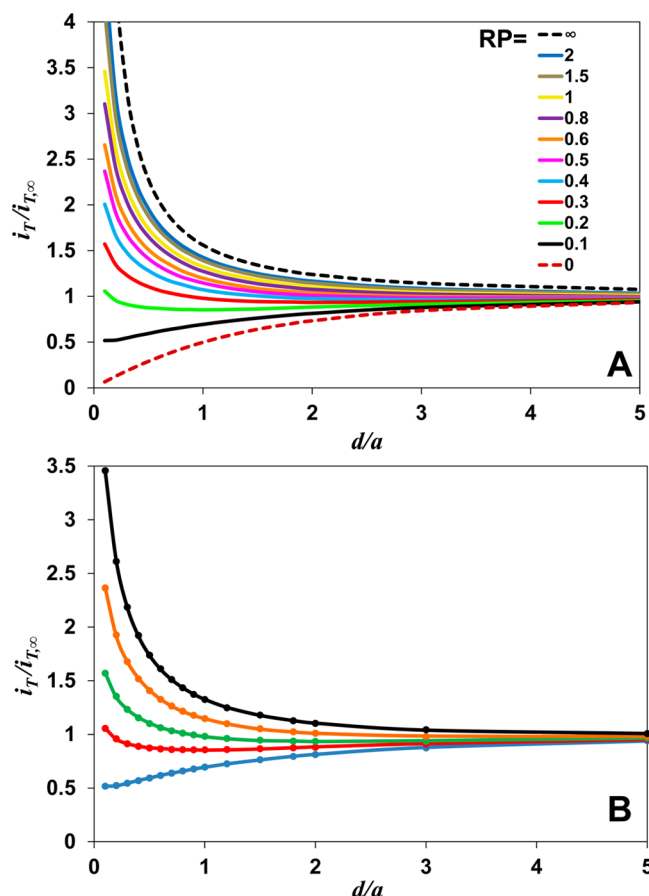


Figure 2. Dimensionless current vs distance curves for a disk-shaped tip with $RG = 10$ approaching a reactive spherical NP immobilized on the inert substrate. (A) The lower and upper dashed curves are for the flat insulating and conductive substrate, respectively. (B) Current–distance curves obtained from simulations (solid lines) and calculated from eq 12 (symbols). From top to bottom, $RP = 1, 0.5, 0.3, 0.2$, and 0.1 .

with the parameter values listed in Table S2, Supporting Information, for different RP s. The numerical results (symbols) fit eq 12 (solid lines) within 0.5% (Figure 2B).

A practically important case is an NP partially buried into the passivating film assembled on the underlying conductive surface. The NP portion exposed to the solution is shaped as a spherical cap. If the film thickness is $> r_p$, the radius of the base of the exposed cap is less than r_p , and the above theory cannot be used to calculate the SECM approach curves. If the film thickness equals r_p , the exposed reactive surface is hemispherical. The approach curves to such a hemisphere were simulated for two different RP values and compared to those obtained at a fully exposed spherical NP (Figure 3). When the NP is relatively large (e.g., $RP \geq 1$), the approach curves simulated for a hemisphere and a full sphere are essentially indistinguishable (cf. blue and red curves calculated for $RP = 1$ in Figure 3). The reason for this similarity is that the positive SECM feedback is mostly produced at the top half of the spherical particle. The blocking effect of the insulating film is not significant in this case because it is mostly screened by the large RP , and the tip never comes close to it. When RP is significantly less than one (e.g., 0.5 in Figure 3), the feedback current at the hemispherical substrate (green curve) is somewhat lower than at the spherical NP (black curve). For

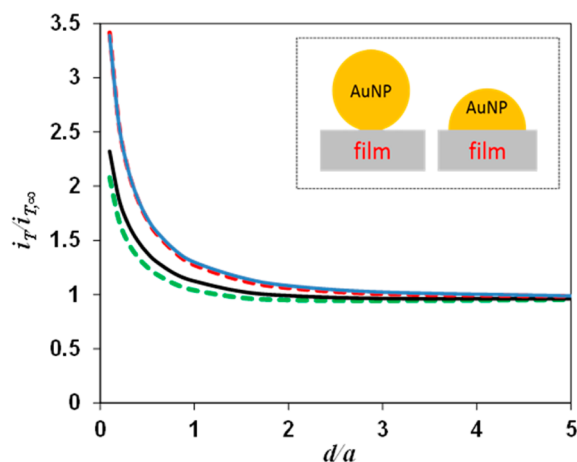


Figure 3. Current–distance curves simulated for a disk-shaped tip approaching equally sized spherical (blue and black solid curves) and hemispherical (red and green dashed curves) reactive NPs attached to the insulating plane. $RP = 1$ (blue and red) and 0.5 (black and green). The inset shows geometries of the fully exposed and partially buried NPs.

$RP = 0.5$, this difference would result in $<20\%$ error in the NP radius value determined by fitting an experimental approach curve to the theory (see below).

Another feature of the above model that is hard to fully implement in the SECM experiment is a perfect positioning of the tip over the center of the surface bound NP. The effect of the lateral shift of the tip center with respect to that of the spherical NP on the shape of SECM approach curves is investigated in Figure 4. Solid lines in Figure 4 were obtained

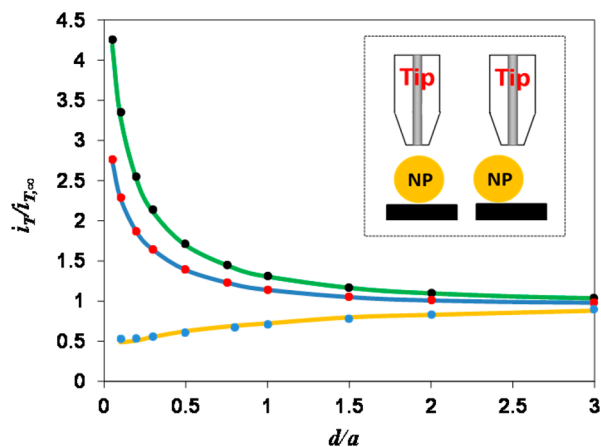


Figure 4. Simulated current–distance curves for the tip center perfectly aligned with that of the reactive spherical NP (symbols) or shifted from it laterally by $0.25a$ (solid lines). $RP = 1$ (black symbols and green line), 0.5 (red symbols and blue line), and 0.1 (blue symbols and orange line). The inset illustrates the perfect (left) and imperfect (right) tip/NP alignment.

by numerically solving the 3D steady-state diffusion problem for the lateral tip displacement equivalent to 25% of its radius ($0.25a$), while symbols represent current–distance curves calculated for the perfectly aligned tip and NP (cf. the left and right pictures in the inset). Figure 4 shows that the approach curves obtained with the $0.25a$ displacement, which represents the experimentally attainable precision of the tip positioning, are practically indistinguishable from the corre-

sponding curves simulated for the perfect tip/NP alignment. The error in the determined RP value associated with the imperfect lateral alignment should be $\ll 10\%$ as long as the displacement is within $0.25a$.

Finding and imaging a small ($RP \ll 1$) reactive NP immobilized on a conductive substrate without breaking the tip is very difficult. Figure 5 contrasts the simulated approach

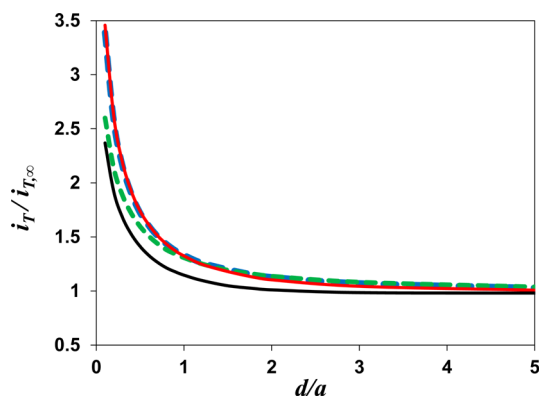


Figure 5. Current–distance curves simulated for a disk-shaped tip approaching a reactive spherical NP immobilized on the conductive (dashed lines) or insulating (solid lines) flat surface. $RP = 1$ (dashed blue and solid red curves) and 0.5 (dashed green and solid black curves).

curves at reactive NPs immobilized on conductive (dashed lines) and insulating (solid lines) substrates. If the NP is relatively large (e.g., $RP \geq 1$), it screens the underlying surface from the tip, and the differences between the curves obtained at a conductive (red solid curve) and insulating (blue dashed curve) support are minor. In contrast, when a smaller NP (e.g., $RP = 0.5$) is immobilized on the conductive surface, significantly higher positive feedback is expected than that obtained with the same particle attached to the insulating support (cf. dashed green and solid black curves in Figure 5). In the cases of relatively large particles (e.g., $RP = 1$), the approach curves (red solid line and dashed blue line in Figure 5) are essentially independent of the substrate nature. Importantly, the effect of the RP on the shape of the approach curve is much smaller when the underlying surface is conductive (cf. dashed green and blue curves). Therefore, SECM is not a promising technique for evaluating the size of a reactive NP attached to the conductive substrate.

In the case of an inert sphere immobilized on an insulating substrate, the magnitude of negative feedback reflects the blocking effects of both the NP and underlying plane on the tip current (Figure 6A). When a NP is small, the approach curve (light blue curve in Figure 6A) is similar to that obtained at the planar insulating substrate (dashed curve). At larger NPs, the blocking effect is weaker, and the feedback is less negative. However, at $RP > \sim 1.5$, the blocking becomes stronger, and the approach curves at very large NPs (e.g., $RP = 100$, black solid curve in Figure 6A) are again very similar to the response obtained at the flat insulating substrate. This dependence is complicated, and the approach curves simulated for larger NPs tend to cross and cannot be easily distinguished. This observation as well as the difficulties in finding a small inert particle on the insulating surface suggest that characterizing this system by SECM can be problematic.

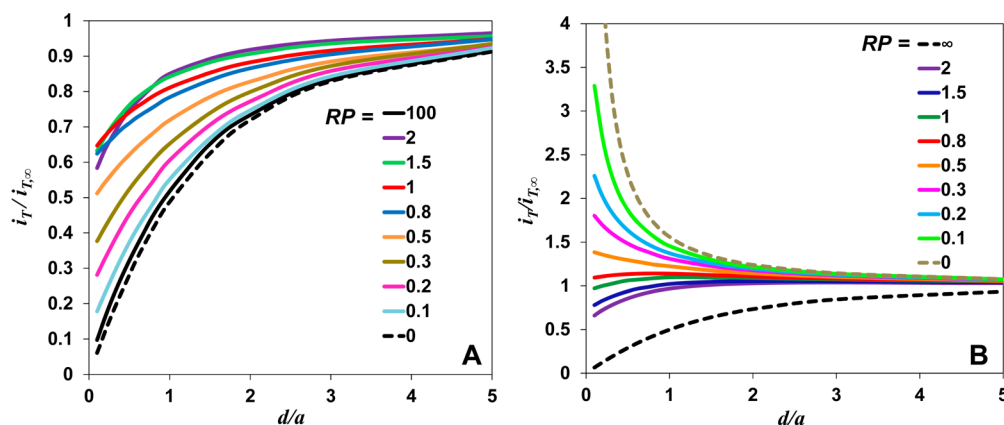


Figure 6. Simulated dimensionless approach curves for inert spherical particles immobilized on the insulating substrate (A) or conductive (B) substrate.

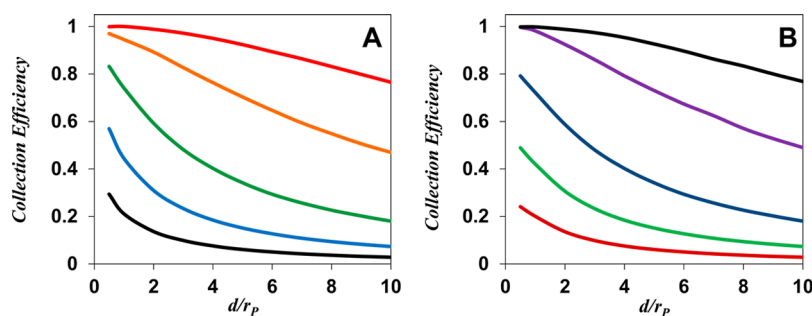


Figure 7. Simulated collection efficiency vs distance dependences for the SG/TC experiment with a spherical substrate. From top to bottom, $RP = 0.1, 0.2, 0.5, 1$, and 2 . The tip electrode regenerates the mediator (A) or produces electroinactive species (B) at a diffusion-controlled rate.

The shape of the current–distance curves for an inert NP immobilized on a conductive substrate strongly depends on the RP value (Figure 6B). For very small NPs (e.g., $RP < 0.1$), the approach curves are essentially identical to that obtained at a flat, uniformly conductive substrate (upper dashed curve in Figure 6B). As the RP increases, the tip current decreases, and the curve shape approaches that of the pure negative feedback (lower dashed curve in Figure 6B). The size of such particles (e.g., droplets or polymer beads²⁹) should be possible to evaluate over the range $\sim 0.2 \leq RP \leq \sim 1$.

SG/TC Mode. In substrate generation/tip collection (SG/TC) mode of the SECM operation, a larger tip collects redox species generated at the NP surface. This approach can be useful for investigating intermediates and mechanisms of electrocatalytic reactions occurring at the NP surface.¹⁷ The steady-state diffusion problem for the SG/TC mode experiment with a finite-size spherically shaped conductive substrate is formulated in the Supporting Information. If the tip process is diffusion controlled and the species produced at the substrate is stable on the experimental time scale, the collection efficiency (i.e., i_T/i_S) is determined by two dimensionless parameters: the normalized separation distance (d/r_p) and the ratio of the particle and tip radii (RP). Figure 7 shows the collection efficiency vs distance dependences for various RP values. The shorter tip–substrate distances and larger tip size (small RP) correspond to higher collection efficiency. Unlike the feedback mode, the distance scale in SG/TC experiments is determined by r_p rather than a . The two panels in Figure 7 represent two typical experimental situations: (A) a reversible process in which the tip regenerates the redox mediator present in the bulk solution at the diffusion-controlled rate and (B) an

irreversible process with the tip producing electroinactive species.

EXPERIMENTAL SECTION

Materials. Ferrocenemethanol (FcMeOH, 97%, Alfa Aesar) was sublimed before use. 4-Aminobenzylamine (99%), NaNO_2 (99.99%), KCl (99%), and HCl were purchased from Sigma-Aldrich and used as received. ZYB grade highly oriented pyrolytic graphite (HOPG) was obtained from K-Tek. Unconjugated AuNPs (Ted Pella, Inc.) were either 20 nm in diameter (7×10^{11} particles/mL) or 100 nm in diameter (5.6×10^9 particles/mL), as specified by the vendor, stabilized with the net negative surface charge by trace amounts of citrate. All aqueous solutions were prepared using deionized water with total organic carbon (TOC) ≤ 5 ppb from the Milli-Q Advantage A10 system equipped with Q-Gard T2 Pak and a Quantum TEX cartridge.

Electrodes and Voltammetry. Polished disk nanoelectrodes were prepared by pulling 25 μm -diameter annealed Pt wires into borosilicate glass capillaries with a P-2000 laser pipet puller (Sutter Instrument Co.) and polishing under video microscopic control, as described previously.³⁰ Voltammograms were obtained with an EI-400 bipotentiostat (Ensmann Instruments, Bloomington, IN) inside a Faraday cage. The two-electrode setup was used with a 0.25 mm diameter Ag wire coated with AgCl serving as a reference electrode. The substrate surface modification was performed in a three-electrode configuration using a platinum wire as a counter electrode and an Ag/AgCl reference electrode (Bioanalytical Systems).

SECM Setup and Procedures. SECM experiments were carried out using a home-built previously described instrument.¹⁷ The nanoelectrode used as an SECM tip was positioned a few tens of micrometers above the substrate surface. A long-distance video microscope was used to monitor the initial approach of the SECM tip to the substrate. The tip was then brought closer to the substrate in an automated mode until the monitored tip current changed by 10%. The current–distance curves were obtained during the subsequent fine approach. An AuNP immobilized on the substrate was located by positioning the tip $\sim 1.5a$ above the substrate plane and scanning it either in X or Y direction while monitoring the tip current. All experiments were carried out at room temperature (23 ± 2 °C) inside a Faraday cage.

AFM and TEM Imaging. An XE-120 scanning probe microscope (Park Systems) was employed for imaging the nanoelectrodes and the HOPG substrate. PPP-NCHR AFM probes (Nanosensors) were used for noncontact imaging. The procedures for AFM imaging of nanoelectrodes were reported previously.³¹ Transmission electron microscopy (TEM) images were obtained using a JEOL JEM-2100 TEM with samples supported on 400 mesh copper grids coated with Formvar/carbon film (Ted Pella, Inc.).

Substrate Preparation. A polyphenylene multilayer was formed *in situ* by the reduction of the corresponding diazonium salt, as described previously.^{17,32} Briefly, 1 mL of 50 mM NaNO_2 was added to 5 mL of aqueous solution containing 10 mM 4-aminobenzylamine and 0.5 M HCl while stirring in an ice bath. The electrografting to graphite surface was achieved by applying two potential sweep cycles between 0.3 and -0.5 V vs Ag/AgCl. HOPG was rinsed with deionized water and dipped into 0.5 M HCl for 1 min to protonate $-\text{NH}_2$ groups. The negatively charged citrate-stabilized gold particles were electrostatically attached to the protonated film by immersing HOPG in AuNP colloid solution for 30 min.

RESULTS AND DISCUSSION

Characterization of Nanoparticles. AuNPs were characterized using TEM and AFM. From TEM images of individual, isolated particles (Figure 8A,B), the diameter of the dry commercial AuNPs was either $19.8 (\pm 1)$ nm or $99.5 (\pm 5)$ nm in good agreement with the nominal 20 and 100 nm values specified by the manufacturer.

An XE-120 scanning probe microscope was employed for the noncontact mode topographic imaging of surface-bound AuNPs. From AFM images (Figure 8C,D), AuNPs electrostatically attached to the polyphenylene film are not aggregated and well separated. The 20 and 100 nm AuNPs appear to be 18–20 nm and 95–106 nm in height and 45–50 nm and 180–200 nm in width, respectively. The overestimation of the lateral dimension of the AuNP is caused by the tip convolution effect, as discussed earlier.^{17,25}

Characterization of Nanoelectrodes. The nanoelectrodes were characterized by steady-state voltammetry and AFM imaging, as discussed previously.³¹ Figure 9A shows a noncontact topographic AFM image of a typical ~ 80 nm-radius polished Pt electrode. From the image, one can see that this electrode was essentially flat and well-polished. The conductive surface was recessed into glass by 4 nm, which is only $\sim 1/20$ of a ; such a small recess depth has a negligible effect on the $i_{T,\infty}$ value and the shape of the SECM approach curves.³³ From the diffusion limiting current in the steady-state voltammogram of 1 mM FcMeOH obtained at the same

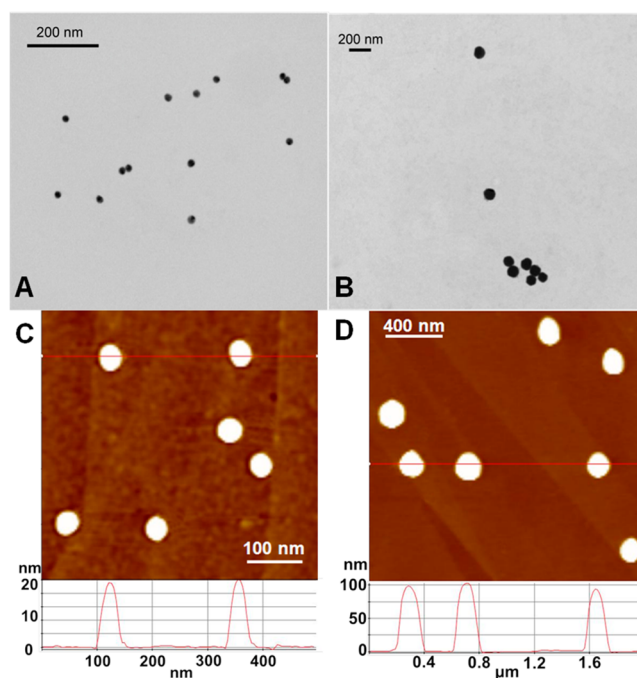


Figure 8. TEM images of 20 nm (A) and 100 nm (B) AuNPs and noncontact topographic AFM images of 20 nm (C) and 100 nm (D) AuNPs immobilized on the HOPG surface modified with a polyphenylene film.

electrode (Figure 9B), the effective radius can be evaluated using eq 11 with $n = 1$, $c^* = 1$ mM, and $D = 7.6 \times 10^{-6}$ cm^2/s ³⁰ for FcMeOH. The effective radius, $a = 79$ nm, obtained from Figure 9B is in agreement with the AFM image in Figure 9A.

Evaluation of the NP Size from SECM Approach Curves. AuNPs attached to the HOPG/polyphenylene film represent the case of a reactive NP on the inert substrate surface.¹⁷ The data in Figure 2 suggest that the particle size can be evaluated by fitting an experimental approach curve to the theory for a broad range of RP values. However, for $RP < 0.2$, the contribution of the positive feedback produced by the particle to the overall current is small, and finding such an NP on the insulating substrate without breaking the tip is difficult. When RP is > 1 , the curve shape is relatively insensitive to its value, and the uncertainty of size determination should be high. Thus, the SECM should be practically suitable for NP measuring for the range of RP values, $\sim 0.2 \leq RP \leq \sim 1$.

The experimental current vs tip displacement curve shown in Figure 10A was obtained with the nanoelectrode that was characterized in Figure 9. When the tip approached an individual AuNP with $r_p = 50$ nm, the current increased, as expected from the theory, and then leveled off abruptly, indicating that the glass sheath of the tip touched the substrate surface. The best fit between this data and the theory was obtained with the RP value of 0.65 (blue solid curve in Figure 10B). Using the tip radius value, $a = 79$ nm, found from the diffusion limiting current and AFM image in Figure 9, $RP = 0.65$ corresponds to $r_p = 51$ nm which agrees very well with the nominal NP radius of 50 nm confirmed by our TEM images (Figure 8A).

The experimental approach curve could be fit to the theory using RP values slightly different from 0.65, e.g., $RP = 0.6$ (orange curve in Figure 10B) or $RP = 0.7$ (red curve). However, no satisfactory fit could be obtained with either $RP =$

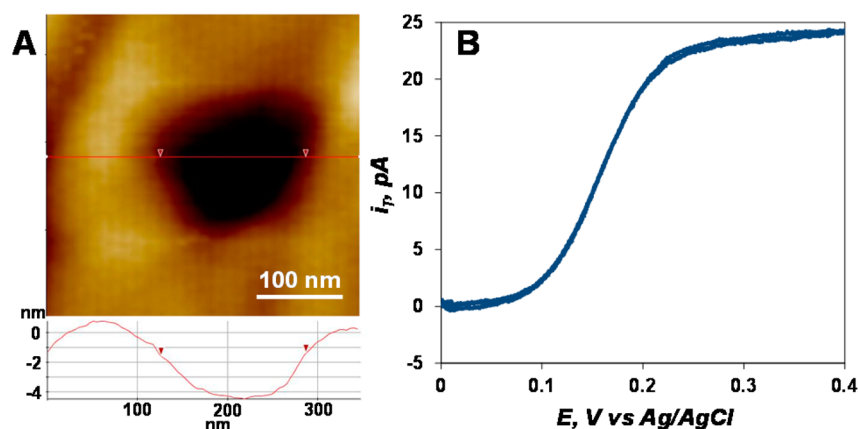


Figure 9. Noncontact topographic image of a 79 nm-radius polished Pt nanoelectrode (A) and a steady-state voltammogram of 1 mM FcMeOH obtained at the same electrode in 0.2 M KCl solution (B).

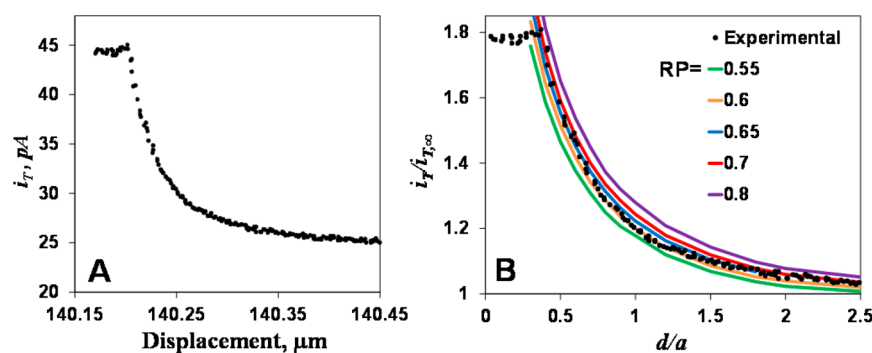


Figure 10. Current vs tip displacement curve obtained with a 79 nm-radius tip approaching a 50 nm-radius AuNP (A) and theoretical approach curves (solid lines) bracketing the experimental data (symbols). (B) Solution contained 1 mM FcMeOH and 0.2 M KCl. The tip current in panel B is normalized with $i_{T,\infty} = 24$ pA.

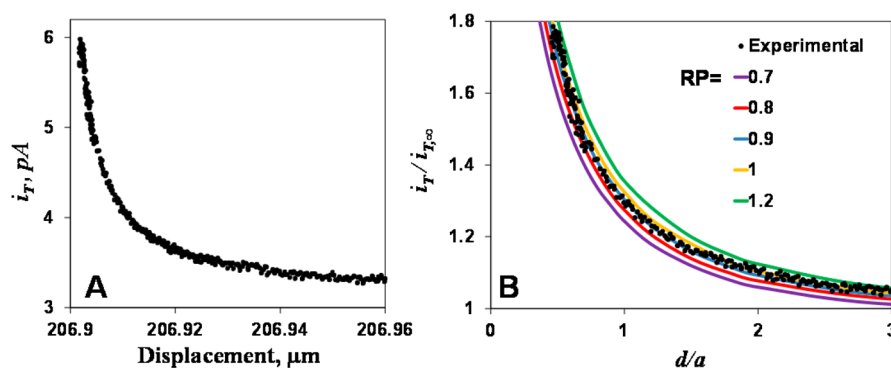


Figure 11. Current vs tip displacement curve obtained with an 11 nm-radius tip approaching a 10 nm-radius AuNP (A) and theoretical approach curves (solid lines) bracketing the normalized experimental data (symbols). (B) Solution contained 1 mM FcMeOH and 0.2 M KCl. $i_{T,\infty} = 3.4$ pA.

0.55 (green curve in Figure 10B) or 0.8 (purple curve). Thus, the $0.6 \leq RP \leq 0.7$ range roughly corresponds to the uncertainty in the NP radius value determined by SECM, $r_p = 51 \pm 5$ nm.

Using a tip with a suitable radius, one can measure much smaller AuNPs (e.g., an NP with the nominal r_p of 10 nm in Figure 11). The current vs tip displacement curve obtained with an 11 nm-radius tip is shown in Figure 11A. For the same data in the normalized form (symbols in Figure 11B), the best fit to the theory was obtained with $RP = 0.9$ (blue curve). The experimental curve in Figure 11B is bracketed by theoretical curves calculated with $RP = 0.8$ (red) and 1 (orange). This data would not fit theoretical curves obtained with either $RP = 0.7$

(purple) or 1.2 (green). The RP range $0.8 \leq RP \leq 1$ corresponds to $r_p = 10 \pm 1$ nm.

CONCLUSIONS

We have developed the SECM theory for a disk-shaped tip approaching a surface-bound spherical particle. Different situations involving either reactive or inert particles immobilized on either conductive or insulating surfaces have been considered. The simulated working curves and a derived analytical approximation can be used to analyze the results of SECM experiments at single nanoparticles. Possible complications such as the imperfect lateral alignment of the tip center with respect to that of the particle and partial burying of a

spherical NP into the insulating surface film have been simulated. The developed substrate generation/tip collection theory is potentially useful for SECM studies of electrocatalytic processes at NPs.

The methodology was developed for evaluating the size of an NP from SECM approach curves. The radii of larger ($r_p = 50$ nm) and smaller ($r_p = 10$ nm) AuNPs attached to the HOPG/polyphenylene substrate were determined by fitting experimental current–distance curves to the theory. The accuracy of such measurements can be affected by inherent nonideality of the nanotip geometry and the uncertainty in the a value determined by steady-state voltammetry, AFM, or other microscopic technique.

■ ASSOCIATED CONTENT

■ Supporting Information

Simulated current vs distance curves, parameter values for eq 12, formulation of the diffusion problem for the SG/TC mode of SECM with a spherical substrate, and COMSOL Model Report. The Supporting Information is available free of charge on the ACS Publications website at DOI: 10.1021/acs.analchem.5b01690.

■ AUTHOR INFORMATION

Corresponding Author

*E-mail: mmirkin@qc.cuny.edu. Fax: 718-997-5531.

Notes

The authors declare no competing financial interest.

■ ACKNOWLEDGMENTS

The support of this work by the National Science Foundation (CHE-1300158) and AFOSR MURI (FA9550-14-1-0003) is gratefully acknowledged.

■ REFERENCES

- (1) (a) Murray, R. W. *Chem. Rev.* **2008**, *108*, 2688–2720. (b) Carducci, T. M.; Murray, R. W. In *Nanoelectrochemistry*; Mirkin, M. V., Amemiya, S., Eds.; CRC Press: Boca Raton, FL, 2015; pp 72–121.
- (2) (a) Kleijn, S. E.; Lai, S. C.; Koper, M. T.; Unwin, P. R. *Angew. Chem., Int. Ed.* **2014**, *53*, 3558–3586. (b) Wang, W.; Tao, N. *Anal. Chem.* **2013**, *86*, 2–14.
- (3) (a) Zamborini, F. P.; Bao, L.; Dasari, R. *Anal. Chem.* **2011**, *84*, 541–576. (b) Welch, C.; Compton, R. *Anal. Bioanal. Chem.* **2006**, *384*, 601–619. (c) Saha, K.; Agasti, S. S.; Kim, C.; Li, X.; Rotello, V. M. *Chem. Rev.* **2012**, *112*, 2739–2779.
- (4) Wieckowski, A.; Savinova, E. R.; Vayenas, C. G. *Catalysis and Electrocatalysis at Nanoparticle Surfaces*; Marcel Dekker: New York, 2003.
- (5) (a) Li, Y.; Cox, J. T.; Zhang, B. *J. Am. Chem. Soc.* **2010**, *132*, 3047–3054. (b) Yamamoto, K.; Imaoka, T.; Chun, W.-J.; Enoki, O.; Katoh, H.; Takenaga, M.; Sonoi, A. *Nat. Chem.* **2009**, *1*, 397–402. (c) Sánchez-Sánchez, C. M.; Solla-Gullón, J.; Vidal-Iglesias, F. J.; Aldaz, A.; Montiel, V.; Herrero, E. *J. Am. Chem. Soc.* **2010**, *132*, 5622–5624. (d) Yang, F.; Zhang, Q.; Liu, Y.; Chen, S. *J. Phys. Chem. C* **2011**, *115*, 19311–19319.
- (6) Perera, N.; Karunathilake, N.; Chhetri, P.; Alpuche-Aviles, M. A. *Anal. Chem.* **2014**, *87*, 777–784.
- (7) Chithrani, B. D.; Ghazani, A. A.; Chan, W. C. W. *Nano Lett.* **2006**, *6*, 662–668.
- (8) Shan, X.; Diez-Perez, I.; Wang, L.; Wiktor, P.; Gu, Y.; Zhang, L.; Wang, W.; Lu, J.; Wang, S.; Gong, Q.; Li, J.; Tao, N. *Nat. Nanotechnol.* **2012**, *7*, 668–672.
- (9) Zhou, X.; Andoy, N. M.; Liu, G.; Choudhary, E.; Han, K.-S.; Shen, H.; Chen, P. *Nat. Nanotechnol.* **2012**, *7*, 237–241.
- (10) Chen, S.; Kucernak, A. *J. Phys. Chem. B* **2003**, *107*, 8392.
- (11) (a) Xiao, X.; Bard, A. J. *J. Am. Chem. Soc.* **2007**, *129*, 9610–9612. (b) Zhou, H.; Park, J. H.; Fan, F.-R. F.; Bard, A. J. *J. Am. Chem. Soc.* **2012**, *134*, 13212–13215. (c) Kim, J.; Kim, B.-K.; Cho, S. K.; Bard, A. J. *J. Am. Chem. Soc.* **2014**, *136*, 8173–8176.
- (12) Zhou, Y.-G.; Rees, N. V.; Compton, R. G. *Angew. Chem., Int. Ed.* **2011**, *50*, 4219–4221.
- (13) Dasari, R.; Robinson, D. A.; Stevenson, K. J. *J. Am. Chem. Soc.* **2013**, *135*, 570–573.
- (14) Sun, P.; Li, F.; Yang, C.; Sun, T.; Kady, I.; Hunt, B.; Zhuang, J. *J. Phys. Chem. C* **2013**, *117*, 6120–6125.
- (15) Guo, Z.; Percival, S. J.; Zhang, B. *J. Am. Chem. Soc.* **2014**, *136*, 8879–8882.
- (16) Yu, Y.; Gao, Y.; Hu, K.; Blanchard, P.-Y.; Noël, J.-M.; Nareshkumar, T.; Phani, K. L.; Friedman, G.; Gogotsi, Y.; Mirkin, M. V. *ChemElectroChem* **2015**, *2*, 58–63.
- (17) Sun, T.; Yu, Y.; Zacher, B. J.; Mirkin, M. V. *Angew. Chem., Int. Ed.* **2014**, *53*, 14120–14123.
- (18) (a) Mirkin, M. V.; Wang, Y. In *Scanning Electrochemical Microscopy*, 2nd ed.; Bard, A. J., Mirkin, M. V., Eds.; CRC Press: Boca Raton, FL, 2012; pp 75–125. (b) Mirkin, M. V.; Fan, F.-R. F.; Bard, A. J. *J. Electroanal. Chem.* **1992**, *328*, 47–62. (c) Selzer, Y.; Mandler, D. *Electrochem. Commun.* **1999**, *1*, 569–575. (d) Selzer, Y.; Mandler, D. *Anal. Chem.* **2000**, *72*, 2383–2390. (e) Daniele, S.; Bragato, C.; Ciani, I.; Baldo, M. A. *Electroanalysis* **2003**, *15*, 621–628. (f) Nann, T.; Heinze, J. *Electrochim. Acta* **2003**, *48*, 3975–3980. (g) Lindsey, G.; Abercrombie, S.; Denuault, G.; Daniele, S.; De Faveri, E. *Anal. Chem.* **2007**, *79*, 2952–2956. (h) Daniele, S.; Ciani, I.; Battistel, D. *Anal. Chem.* **2008**, *80*, 253–259.
- (19) (a) Fulian, Q.; Fisher, A. C.; Denuault, G. *J. Phys. Chem. B* **1999**, *103*, 4387–4392. (b) Fulian, Q.; Fisher, A. C.; Denuault, G. *J. Phys. Chem. B* **1999**, *103*, 4393–4398.
- (20) (a) Sklyar, O.; Wittstock, G. *J. Phys. Chem. B* **2002**, *106*, 7499–7508. (b) Sklyar, O.; Träuble, M.; Zhao, C.; Wittstock, G. *J. Phys. Chem. B* **2006**, *110*, 15869–15877.
- (21) (a) Vogel, R.; Willmott, G.; Kozak, D.; Roberts, G. S.; Anderson, W.; Groenewegen, L.; Glossop, B.; Barnett, A.; Turner, A.; Trau, M. *Anal. Chem.* **2011**, *83*, 3499–3506. (b) German, S. R.; Hurd, T. S.; White, H. S.; Mega, T. L. *ACS Nano* **2015**, DOI: 10.1021/acs.nano.5b01963.
- (22) (a) Terejanský, P.; Makra, I.; Fürjes, P.; Gyurcsányi, R. E. *Anal. Chem.* **2014**, *86*, 4688–4697. (b) White, H. S., private communication.
- (23) Gomez, M. V.; Guerra, J.; Myers, V. S.; Crooks, R. M.; Velders, A. H. *J. Am. Chem. Soc.* **2009**, *131*, 14634–14635.
- (24) Liu, L.; He, B.; Liu, Q.; Yun, Z.; Yan, X.; Long, Y.; Jiang, G. *Angew. Chem., Int. Ed.* **2014**, *53*, 14476–14479.
- (25) Zheng, J.; Zhu, Z.; Chen, H.; Liu, Z. *Langmuir* **2000**, *16*, 4409–4412.
- (26) Ebenstein, Y.; Nahum, E.; Banin, U. *Nano Lett.* **2002**, *2*, 945–950.
- (27) (a) Zhao, J.; Bradbury, C. R.; Huclova, S.; Potapova, I.; Carrara, M.; Fermin, D. J. *J. Phys. Chem. B* **2005**, *109*, 22985–22994. (b) Chazalviel, J.; Allongue, P. *J. Am. Chem. Soc.* **2010**, *133*, 762–764.
- (28) Bard, A. J.; Mirkin, M. V.; Unwin, P. R.; Wipf, D. O. *J. Phys. Chem.* **1992**, *96*, 1861–1868.
- (29) (a) Boika, A.; Thorgaard, S. N.; Bard, A. J. *J. Phys. Chem. B* **2013**, *117*, 4371–4380. (b) Kim, B.-K.; Boika, A.; Kim, J.; Dick, J. E.; Bard, A. J. *J. Am. Chem. Soc.* **2014**, *136*, 4849–4852.
- (30) Sun, P.; Mirkin, M. V. *Anal. Chem.* **2006**, *78*, 6526–6534.
- (31) Nogala, W.; Velmurugan, J.; Mirkin, M. V. *Anal. Chem.* **2012**, *84*, 5192–5197.
- (32) (a) Belanger, D.; Pinson, J. *Chem. Soc. Rev.* **2011**, *40*, 3995–4048. (b) Anariba, F.; DuVall, S. H.; McCreery, R. L. *Anal. Chem.* **2003**, *75*, 3837–3844.
- (33) Sun, P.; Mirkin, M. V. *Anal. Chem.* **2007**, *79*, 5809–5816.